Numerical modelling of the mechanical behaviour of Aluminosilicate Glass: A comparison between two simulation approaches

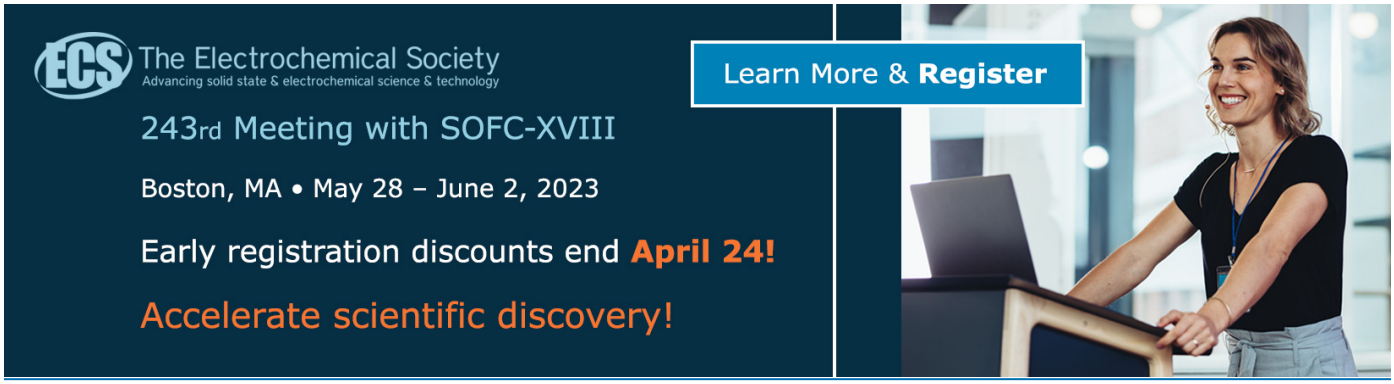

Numerical modelling of the mechanical behaviour of Aluminosilicate Glass: A comparison between two simulation approaches

A Manes[1*], M N Tartaglia[1] and Z Wang[2]

[1] Politecnico di Milano, Department of Mechanical Engineering, Milan 20156, Italy
[2] Faculty of Materials and Manufacturing, Beijing University of Technology, Beijing 100124, China

Email: andrea.manes@polimi.it

Abstract. This paper presents a comparison between two numerical methods for modelling the mechanical and failure behaviour of aluminosilicate glass: Cohesive Elements Method (CEM) and Finite Element Method coupled to Smooth Particle Hydrodynamics (FEM-SPH). The failure behaviours, provided by these two approaches, are herein compared under i) quasi-static tests on material coupons, ii) dynamic tests (compressive and tensile tests) also on material coupons and iii) structural impact loading conditions in which the ballistic perforation of aluminosilicate glass tiles due to the impact of a flat-nosed steel projectile are considered. Both methods provide comparable results under quasi-static loading conditions, while more significant differences arise in the ballistic impact part, in which some limitations of CEM are shown.

1. Introduction

Aluminosilicate glass is a brittle material widely employed as windshields of vehicles, aircrafts, and also transparent touchscreens of electronic devices like smartphones and tablets. [1] Thanks to the presence of about 20% of Aluminum oxide in the composition of the material, Aluminosilicate glass possesses higher mechanical strength and chemical stability with respect to soda-lime glass. In general, the mechanical properties of Aluminosilicate glass differ quite a lot in compression and in tension loading conditions. As the compression strength and hardness are relatively high, the main weaknesses of the Aluminosilicate glass are its low tensile strength and its failure mechanisms characterized by large fragmentation. Accordingly, better understanding of the failure properties of the material under different loading conditions is necessary for accurate design of a component made of this material. Considering the efforts required to perform real experimental tests and the complex failure mechanism, the development of reliable numerical models able to predict the behaviour of glass structures under different loading conditions would simplify this task.

Studying the behaviour of a loaded glass structure is not simple and, especially, due to the complexity of crack patterns, the large number of factors the failure behaviour depends on (concentration of defects inside the material, stress state, loading speed, temperature, geometry, etc.) and the discontinuity of the failure process (crack initiation, propagation, branching and failure). All these factors make the prediction of the failure behaviour very challenging and complicated to be performed both in qualitative and quantitative terms.

Finite Elements Method (FEM) remains one of the most used numerical methods for the analysis of stresses and strains due to its capability to mimic complex and specific physical behaviour and its calculation efficiency. However, in the analysis of non-linear problems such as failure simulation, some drawbacks arise [2]. In fact, FEM alone is quite unsuitable for the description of both cracking and fragmentation processes. Element erosion is a common choice to represent the formation of cracks in brittle solids inside the FEM framework. Element erosion implies that when an element of the model reaches the failure limit, according to a certain failure criterion, it is handled differently with respect to the remaining non-eroded elements. Several algorithms that handle failed elements exist, but usually eroded elements are either deleted and removed from the calculations, or, alternatively, their stresses are set to zero. However, such an operation is clearly unphysical since it involves the sudden disappearance of a part of the material and, thus, is associated with mass and energy loss [3]. Even if this approach may deliver reasonable results for a limited extent of failure, it becomes impractical for the reproduction of large fragmentations. Following these considerations, two approaches are herein considered by the authors to overcome this problem:

1. The insertion of Cohesive Elements in-between all the solid elements.
2. The transformation of the failed solid elements into Smooth Particle Hydrodynamics particles.

The Cohesive Elements Method (CEM) consists in the insertion of a zero-thickness solid element at the interface between every couple of elements (independent of their shape). Such an added element (which is properly a cohesive element) has different properties from the bulk material, but rather possesses the properties of the process zone ahead of the crack tip, following the Cohesive Zone Model theory by Dugdale and Barenblatt [4,5]. When a cohesive element reaches a certain loading condition (described by a cohesive law), the element is deleted, leaving the neighbouring solid elements as separated elements. Consequently, a realistic situation is reached, in which a disconnection between two neighboring solid elements, left by the deleted cohesive element, is formed. This disconnection represents the formation of a crack. Being zero-thickness, the deletion of cohesive elements does not cause any kind of mass or energy loss. A work by Pandolfi and Ortiz [6] used this technique with the aim to reproduce the tridimensional fragmentation of brittle materials in a three-point bending test. In other works, the fragmentation of rocks [5,7] and glass [3,8] was studied. However, very few studies on the ballistic impact of glass are present in the literature.

Pure Smooth Particle Hydrodynamics (SPH) is one of the earliest meshless method available and one of the most popular for a wide range of applications. SPH has proven to be effective in modelling the fracture of brittle materials [9–11]. In fact, lacking a predefined connection between nodes, this simulation technique predicts the behaviour of non-continuum materials well, like pieces of glass after failure. However, even though the SPH method is generally more suitable, efficient, and robust for problems involving severe distortions, its accuracy, stability, and efficiency is not as good as that of FEM for problems with mild distortions [12]. For this reason, the idea of investigating the feasibility of using traditional finite elements for the field of small distortion and eventually convert element subjected involved into large distortion into SPH particles. The newly generated SPH particles inherit all the mechanical properties of the eroded solid elements, including mass, energy, and constitutive properties. Thereby in a hybrid method the benefits of the classical FEM (easiness, fastness, simplicity) and the pure SPH method (conservation of mass and energy, good reproduction of pulverization of brittle materials) can be combined.

In this paper the Cohesive Elements Method (CEM) and the FEM-SPH (Finite Element coupled to Smooth Particle Hydrodynamics) simulation techniques were employed to run comparative analyses about compressive, tensile and impact behaviour of Aluminosilicate glass. Specifically, a Uniaxial Compression model and a Brazilian Disc Tensile model were used to calibrate and verify the two numerical techniques in different loading conditions, according to the experimental results. Finally, a numerical ballistic impact model was built to test the capability of the two methods to simulate the mechanical behaviour of Aluminosilicate glass. All calculations present in this work were developed on the commercial software LS-DYNA.

2. Materials and experimental results

2.1. Material description

Aluminosilicate glass is a kind of inorganic silicate glass that contains 15% to 25% aluminum oxide. This addition leads to an increase of the mechanical properties in terms of hardness and strength. In Table 1 the detailed chemical composition of Aluminosilicate glass is listed.

Table 1. Chemical composition of Aluminosilicate glass specimens considered in this work.

Oxides	SiO_2	Al_2O_3	Na_2O	MgO	K_2O	CaO	Others
Wt%	64,3	17,7	10,4	3,8	2,5	0,5	0,8

2.2. Specimens and experiments

All experimental data used herein were taken from previous works by Wang et al. [1] and no experimental activity was specifically conducted for the present work. The experimental data include the quantitative results for Uniaxial Compression, Brazilian Disc Tension and Flat-nosed projectile ballistic impact tests. These values are meaningful to provide a quantitative overview of the compressive and tensile properties as well as the impact response of the glass structure. The detailed geometry of the used specimens is shown in Figure 1. The quantitative results of the experimental tests are listed in Table 2.

Table 2. Material's mechanical properties under different loading conditions.

Loading condition	Loading Speed (mm/s)	Elastic Modulus (GPa)	Failure Strength (MPa)	Failure Strain
Uniaxial Compression	0,032	77,3 ± 10,9	579,22 ± 52,48	$8{,}31{\cdot}10^{-3}$ ± 0,0009
	1600	75,9 ± 27,5	897,03 ± 45,47	$1{,}32{\cdot}10^{-2}$ ± 0,0020
	3200	76,6 ± 27,2	1073,53 ± 66,66	$1{,}42{\cdot}10^{-2}$ ± 0,0005
Brazilian Disc Tension	0,002	59,2 ± 5,0	44,25 ± 8,15	$7{,}50{\cdot}10^{-4}$ ± 0,0002
	4000	61,3 ± 6,4	81 ± 11,92	$1{,}35{\cdot}10^{-3}$ ± 0,0003

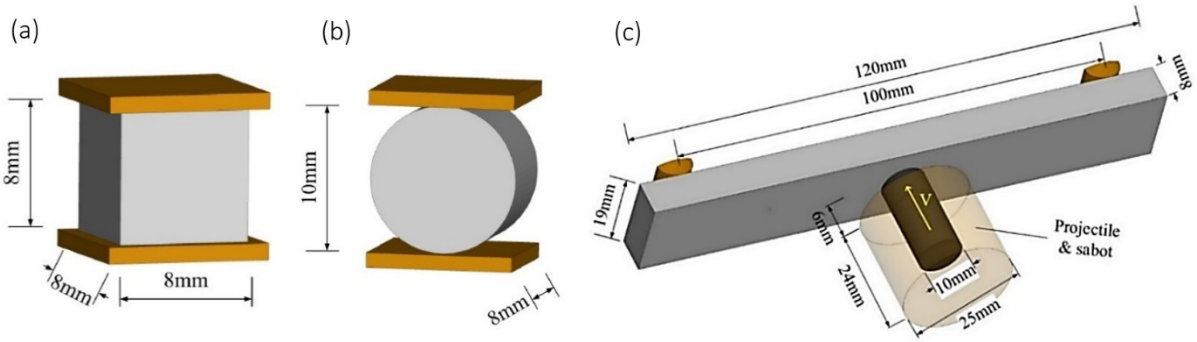

Figure 1. Sketch of the specimens' geometries: (a) Uniaxial Compression, (b) Brazilian Tension, (c) Ballistic Impact.

3. Numerical analyses

In order to develop a reliabl model for the prediction of the impact behaviour of Aluminosilicate glass, a Uniaxial Compression model and a Brazilian Disc Tensile model were built to calibrate and verify the two numerical techniques under different loading conditions (specifically, respectively under compressive and tensile loadings). The aim of this part was to trace the limits of validity of the considered numerical methods, in terms for instance of mesh size, mesh geometry and application of the

loads. These are fundamental data for the correct development of a reliable model, able to provide realistic results in a wide range of situations.

3.1. Cohesive Element Method

3.1.1. Numerical model

For all the numerical models making use of CEM, only two types of material' models were employed: solid elastic elements for Aluminosilicate glass specimens and steel plates (whenever they were present) and cohesive elements in-between the solid ones. The default constant stress solid element defined in LS-Dyna by ELFORM=1 was considered for solid elements. Instead, ELFORM=19 elements were used as cohesive elements. They are flat zero-thickness 8-node solid elements with 4 integration points.

These elements were given the following materials' models in LS-Dyna: 001_Mat_Elastic for glass solid elements, 020_Mat_Rigid for the elements belonging to the steel parts and 138_Mat_Cohesive_Mixed_Mode or 184_Mat_Cohesive_Elastic for cohesive elements. The materials models' parameters are listed in Table 3. The properties of steel and Aluminosilicate glass were taken respectively from references [13] and [14].

Table 3. Materials parameters used in CEM analyses.

Steel 020_Mat_Rigid	Density	ρ	7,8	g/cm^3
	Elastic Modulus	E	210	GPa
	Poisson Ratio	ν	0,31	
Aluminosilicate Glass 001_Mat_Elastic	Density	ρ	2,546	g/cm^3
	Elastic Modulus	E	75	GPa
	Poisson Ratio	ν	0,22	
Cohesive Elements 138_Mat_Cohesive Mixed_Mode	Density	ρ	2,546	g/cm^3
	Stiffnesses in/normal to the plane of the cohesive element	E_T	1e+04	GPa/mm
		E_N	1e+04	GPa/mm
	Peak traction in normal/tangential direction	T	45	MPa
		S	225	MPa
	Energy release rate for mode I and mode II	G_{IC}	0,02	MPa/mm
		G_{IIC}	0,1	MPa/mm
	Ultimate displacements in normal/tangential direction	UND	0,002	mm
		UTD	0,002	mm
	Exponent of the model	XMU	1	
Cohesive Elements 184_Mat_Cohesive Elastic	Density	ρ	2,546	g/cm^3
	Stiffness in/normal to the plane of the cohesive element	E_T	1e+04	GPa/mm
		E_N	1e+04	GPa/mm
	Peak traction in normal/tangential direction	FN_FAIL	45	MPa
		FT_FAIL	225	MPa

For cohesive elements, a previous work by Wang et al. was considered [3], however the values of T and FN_FAIL were set equal to the maximum tensile strength of Aluminosilicate glass and the value of S and FT_FAIL were five times larger than T, as stated in the citated paper.

In the simulation of Uniaxial compression and Brazilian tension, two possible configurations of models were built with or without the compressing plates. In either case, the parts corresponding to the solid and cohesive elements of the specimens were always considered as a unique set of parts. For this reason, for the models in which the pressing steel plates were present, the AUTOMATIC_SURFACE_TO_SURFACE contact option was used, in which a contact between the plates and a set of parts (glass solid elements and cohesive elements) was imposed and the upper plate was subjected to a displacement-controlled loading scheme. Conversely, in the models without the presence of pressing plates, all the constraints of the boundary conditions were applied directly onto sets of nodes positioned at the top and bottom of the specimen.

When the LS-DYNA/Explicit solver is used for quasi-static loading conditions, the numerical loading time must be long enough to avoid dynamic effects, which can cause stress wave propagation in the specimen and dynamic oscillations in the loading curves. However, a longer loading time results in higher computational cost. Different loading times were, thus tried and the loading speed of 100 mm/s was used for the quasi-static simulations to obtain both good simulation results and acceptable computational efficiency.

3.1.2. Analyses and results

Several investigations were conducted using CEM both on the Uniaxial Compression model (UC) and Brazilian Disc Tensile model (BDT) to test the feasibility of this technique. Accordingly, the predefined displacement loading was applied through two steel compressive plates. To avoid non-negligible fragmentation of the elements situated in contact between the specimen and the plates due to stress concentration, two modifications were performed on the model:

1. Modification of the geometry of the specimen, in order to flatten and enlarge the contact surfaces
2. Introduction of some stronger cohesive elements near the contact zone, with the aim of reinforcing the contact area and reducing the effects of stress concentration

It was possible to employ stronger cohesive elements due to the fact that in Brazilian discs failure starts from the central part of the specimen and then propagates towards the contact areas. Hence, no direct contribution of the added stronger elements to the strength of the specimen can be expected. Specifically, the inserted values for T and S cards (peak traction values in normal and tangential direction) of the stronger cohesive elements were typically two or three times larger than those indicated in Table 3.

In Figure 2 a representation of a so-obtained Brazilian Disc Tensile model is shown. In particular, in the image on the right a representation of the model after having hidden the solid elements of the specimen is reported. As can be imagined, the remaining finite elements of the disc are only the cohesive elements. Due to their null thickness, they were not visible in the complete representation with all the elements of the model. The brown parts (near the contact zone) represent the stronger cohesive elements' part.

With this BDT model, the behaviour of different cohesive models was firstly explored. In fact, different cohesive models are present in LS-Dyna, such as Mat_138 (Cohesive Mixed Mode) and Mat_184 (Cohesive Elastic), differing in their cohesive law. The aim of this preliminary investigation was to explore the upper mesh size limit for the material's model below which a convergence of results could be obtained. The analysis was performed by building several models with different mesh sizes to identify at which point the desired output quantities (for instance strength and maximum strain) converge to the same value. Here three output quantities were considered for the comparison:

1. Maximum reaction force
2. Maximum normal stress of the firstly failed cohesive element

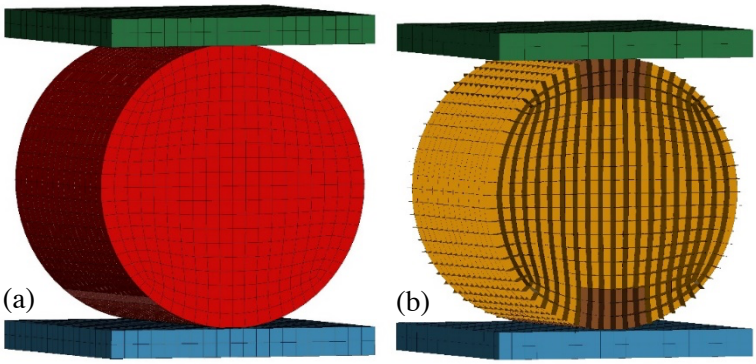

Figure 2. (a) Representation of the obtained Brazilian Disc Tensile model. (b) Representation of the model in which the cohesive elements (yellow and brown) are the only elements belonging to the specimen that are left visible.

The first analysis consists in the representation of the maximum reaction force exhibited by each models using different mesh sizes. In a similar way, the maximum normal stress of the first cohesive element reaching the failure condition was used as output magnitude to explore the mesh sensitivity of the models. In this analysis, for several models with different mesh sizes, the first cohesive element to reach the imposed deletion condition was retraced and its maximum stress directed orthogonally with respect to its plane (also referred to as "Z-Stress") was inserted in the diagram with the corresponding mesh size. These two analyses were useful to determine the dependence of each material's model on the mesh size and the plots obtained are reported in Figure 3. As visible the CEM models revealed not to be mesh size sensitive in tension (BDT).

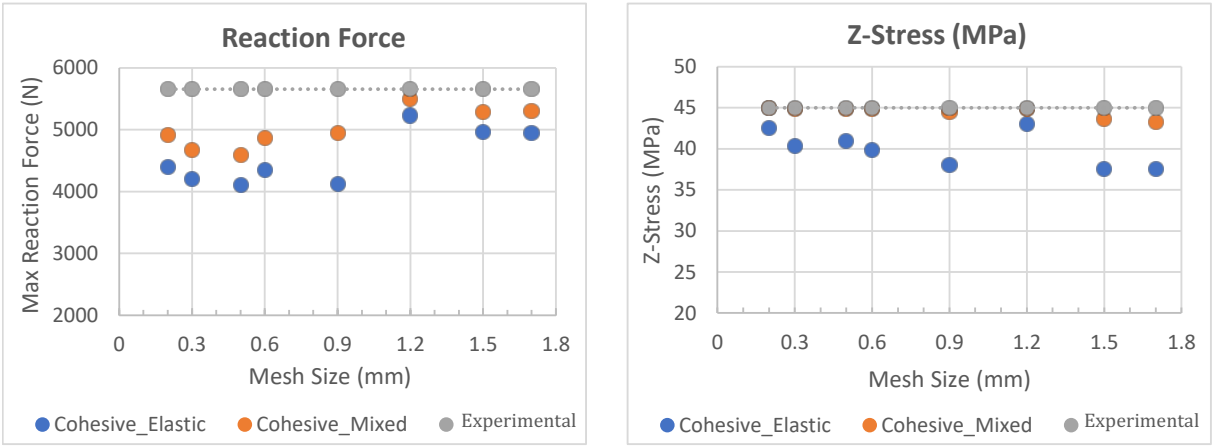

Figure 3. BDT simulations: comparison of the mesh size sensitivities of Cohesive_Elastic and Cohesive_Mixed_Mode cohesive models in terms of Maximum Reaction Force and Maximum Orthogonal Stress exiting the plane of cohesive elements ("Z-Stress").

According to the obtained results, Cohesive_Mixed_Mode demonstrated to be the cohesive model that provided the best results. Consequently, this model was employed for further analyses, including a further mesh size sensitivity, mesh geometry dependence and strain rate effect.

As highlighted before, no mesh size sensitivity could be outlined under tensile loading conditions for CEM. In an analogous way, the dependence from mesh size of the UC model was explored by tracing for different mesh sizes the maximum compressive stress determined from the values of maximum reaction force. The loading speed was chosen again equal to 100mm/s. As can be seen in Figure 4, no clear convergence was obtained but, despite some oscillations, a reasonable convergence of results can be noticed for mesh size finer than 0,6mm.

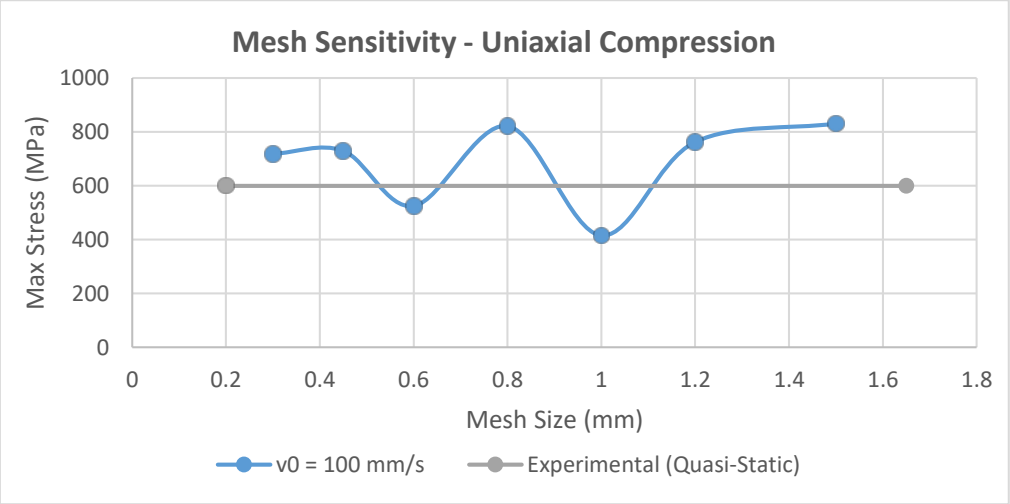

Figure 4. Mesh size sensitivity for the UC model using CEM.

Finally, the possibility to predict the strain rate dependence of Aluminosilicate glass using CEM was explored. In fact, as shown in Table 2, for increasingly higher strain rates, the specimens made with this material increase their strength and the maximum deformation that is reached before failure. The analysis was conducted again in parallel for BDT and UC models with mesh sizes respectively of 1,2 mm and 0,6 mm. It should be pointed out first that the exact quasi-static loading conditions (0,002 mm/s) could not really be reproduced as the corresponding loading speed would result in too long computational time. However, in contrast to the UC model, no strain rate dependence was outlined for the model in tensile loading conditions whereas with the UC model a strain rate effect were obtained for compression behaviour. The trends of the maximum stress and maximum strain are reported in Figure 5 and the numerical values were compared with experimental ones (already reported in Table 2). As visible, an increase in the maximum stress and strain was clearly detected.

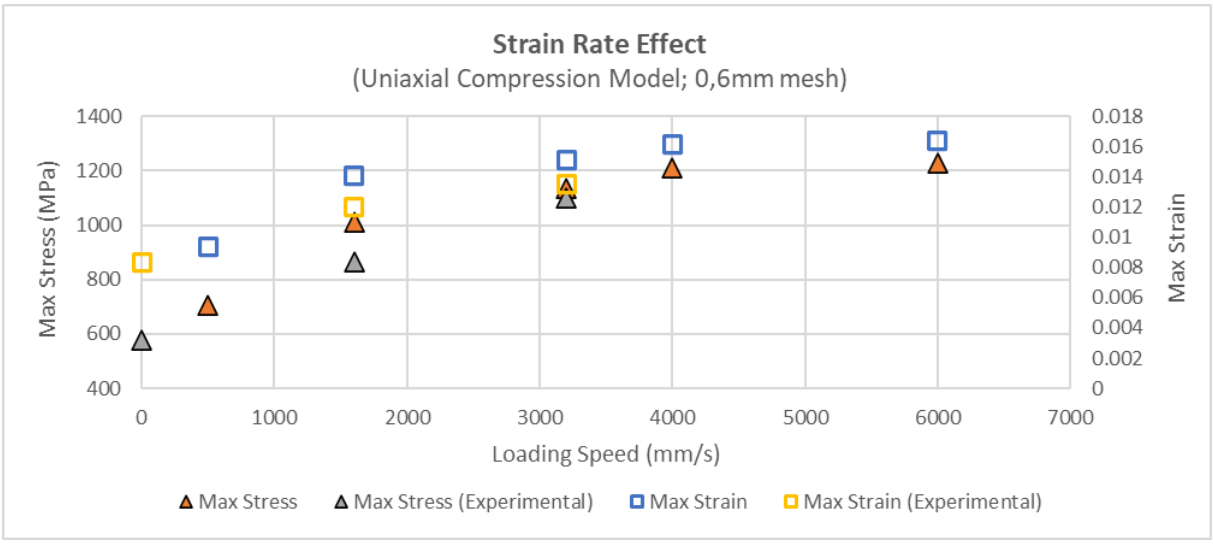

Figure 5. Strain rate dependence of UC model.

These results are not only good in qualitative terms, but also the quantitative results of the experimental tests were confirmed. The most interesting fact is that such a quantitative confirmation of the experimental results was obtained not only without parametrizing the material parameters with

respect strain rate effect, i.e. without inserting any direct loading speed dependence in the constitutive parameters of the material. Such strain rate-dependent numerical strength could be explained by the fact that in the UC specimen multiple cracks initiate and propagate. After the deletion of cohesive elements, the interaction between the glass debris (corresponding in this simulation to the solid elements, remained free and unbounded after the failure of the cohesive elements, but still possessed a certain inertial contribution) provides some contribution to the final strength of the numerical specimen. This contribution was not present in tensile loading conditions, where following the elimination of cohesive elements, solid elements are driven far away from each other by the acting state of stress.

3.2. FEM-SPH

3.2.1. Numerical model

As mentioned above in the FEM-SPH approach the glass specimens were built at first as usual finite element parts and were converted into SPH particles after failure. Such a conversion process is regulated by the definition of the keyword Define_Adaptive_Solid_to_SPH already present in LS-Dyna. There are two user-input parameters ICPL and IOPT related to this keyword that were set equal to 1, meaning that coupling occurs when the solid element fails. Also, every finite element was adapted to one SPH element, by putting the NQ card equal to 1.

The SPH part is defined by the keyword card SECTION_SPH. In the selection of the parameters for the SPH part of the models, the default options were used: CSLH (a constant applied to the smoothing length of the particles) was set equal to 1,2, while the scale factors for the maximum and minimum smoothing length were respectively HMAX = 2 and HMIN = 0,2. Also, the default cubic spline kernel function was used (SPHKERN = 0).

Table 4. JH2 model parameters for Aluminosilicate glass.

Parameter	Notation	Value	Units
Density	ρ_0	2545,62	Kg/m^3
Poisson's Ratio	ν	0,22	
Elastic Modulus	E	75,13	GPa
Equivalent Stress at Hugoniot Elastic Limit	σ_{HEL}	5,95	GPa
Pressure at Hugoniot Elastic Limit	P_{HEL}	3,07	GPa
Maximum hydrostatic tensile stress	$\sigma_{t,max}$	45	MPa
Intact Strength coefficient	A	0,93	
Intact strength exponent	N	0,76	
Strain rate coefficient	C	0,036	
Fractured strength coefficient	B	0,2	
Fractured strength exponent	M	1	
Elastic bulk modulus	K_1	44,72	GPa
Coefficient for 2nd degree term in EOS	K_2	-67,45	GPa
Coefficient for 3rd degree term in EOS	K_3	141,6	GPa
Energy conversion coefficient	β	1	
Damage coefficient	D_1	0,043	
Damage exponent	D_2	0,85	

As far as the FEM part is concerned, the considered parameters are listed in Table 4. In this case, for the FEM part, 110_MAT_Johnson_Holmquist_Ceramics corresponding to Johnson-Holmquist 2 constitutive model [15] (often also abbreviated with JH2) was employed to describe the mechanical behaviour of Aluminosilicate glass before failure. The material parameters were taken from previous works of Wang et al. [1,14].

3.2.2. Analyses and results

The first conducted analysis was a mesh size sensitivity analysis, to find whether and in which conditions the models showed a convergence of results. Furthermore, the possibility to remove the compressing plates was explored for the UC model. The models and the results are shown in Figure 10. For the BDT model a proper mesh size can be outlined, while the UC model is mesh size insensitive. However, the presence of compressing plates decreases the reliability of the model. In the end, a 0,5 mm mesh was used for all remaining analyses, and no investigation on the behaviour of the model without the presence of plates was conducted, gigure 6.

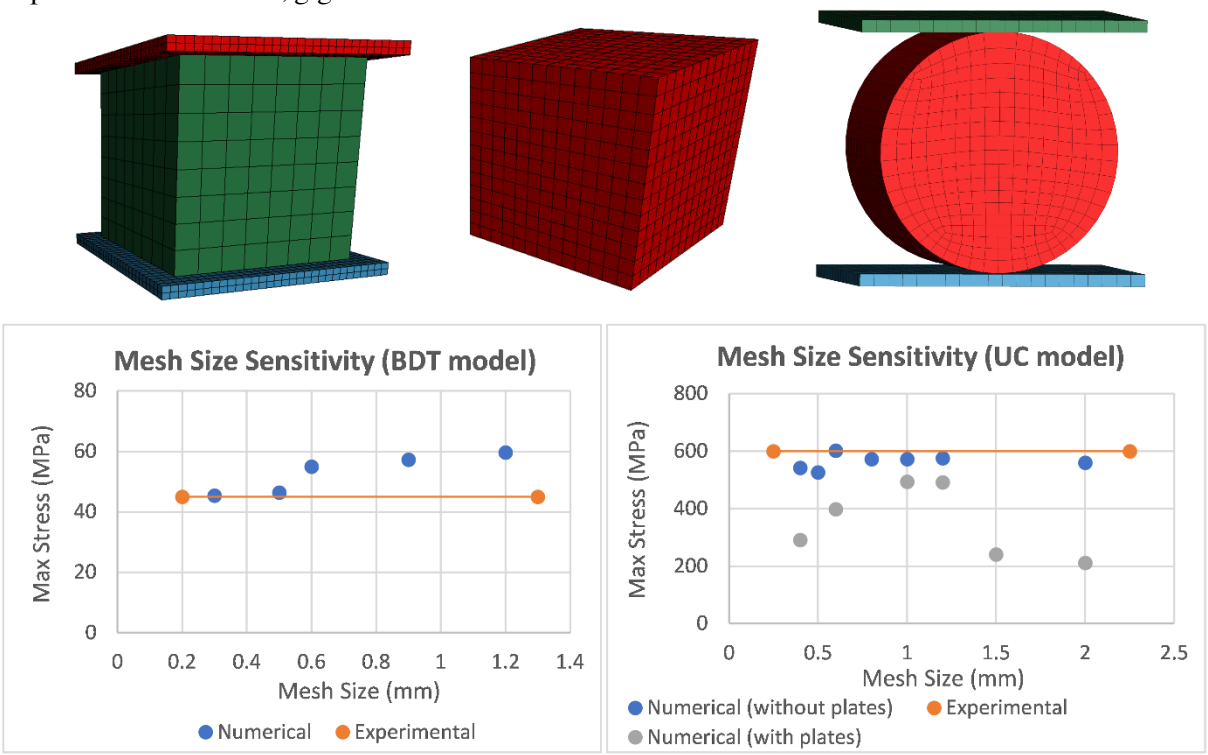

Figure 6. Models for mesh sensitivity analysis and results for FEM-SPH hexahedral mesh.

Different is the case of the strain rate effect. In fact, the strength included in JH-2 model parameter and indicated with the letter C in the constitutive equation in LS-Dyna, directly relates the compressive strength with the strain rate effect of the model. Coherently with this, only UC specimens showed a strain rate dependence in their strengths. As reported in Table 4, a value of 0,036 was calibrated for the parameter. In Figure 7 the strain rate effect of the UC model is depicted.

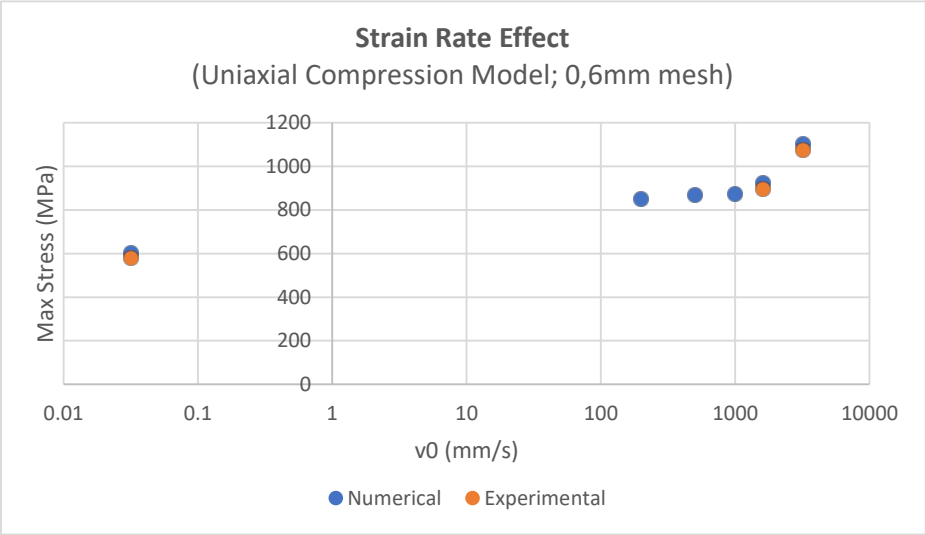

Figure 7. Strain rate effect on the strength of a 0,6mm mesh UC model.

The discussion of the last sections showed the capabilities of CEM and FEM-SPH models. CEM was studied by comparing 184_Cohesive_Elastic and 138_Cohesive_Mixed_Mode cohesive laws and following the demonstration of the Cohesive_Mixed_Mode model's reliability, this cohesive model was selected to investigate, the mesh size sensitivity of the CEM and its capability to predict the strain rate effect. Mesh size dependence above 0,6mm mesh and strain rate sensitivity only in compression were highlighted. Solid elements described by 110_MAT_Johnson_Holmquist_Ceramics constitutive model were used to build tensile and compressive specimens that turned into SPH particles whenever a failure condition was met. This model resulted to be mesh size sensitive in tension for meshes coarser than 0,5 mm and strain rate sensitive in compression. In this framework, for the following structural analysis of impact loadings, the two approaches were tested and compared.

4. Ballistic impact simulation

After having explored the potential of the two simulation techniques to reproduce the behaviour of the material in simple loading conditions, the attention was moved to the simulation of a ballistic impact onto an Aluminosilicate glass tile. The impact behaviour of Aluminosilicate glass was tested experimentally with a flat-nosed steel projectile at two impact velocities: 84 m/s and 139 m/s. A polymeric sabot covering the bullet was adopted to improve the trajectory during the test. The obtained experimental residual speeds of the bullet are 66 m/s and 127 m/s respectively, as shown by Wang et al. [16].

4.1. Numerical model

In this analysis, a glass tile modelled with the two numerical approaches considered so far was impacted by a flat-nosed projectile. In the numerical models, the only part subject to modifications was the glass tile, which was modelled with different mesh sizes (1mm for CEM, 0,5mm for FEM-SPH) and exploiting the two different approaches previously introduced: i) SPH conversion rule ii) cohesive elements embedded between the solid ones. All the remaining parts were kept unchanged and full size models were adopted with dimensions already shown in Figure 1.

The aluminium supporting bars were designed using the simple 001_Mat_Elastic material model with a density of 2,7 g/cm^3, an elastic modulus of 72 GPa and a Poisson ratio of 0,3 (with the consistent units of measure shown in section 4.1). The same material model was used for the polymeric sabot of the projectile (density = 1,13 g/cm^3, elastic modulus = 1,511 GPa, Poisson ratio = 0,3). The properties of the Cohesive elements and FEM-SPH parts were the same as already presented in the previous sections. The carbon steel projectile was modelled using the material model

098_Simplified_Johnson_Cook model (JC) with a mesh size of a 0,15mm. The projectile was put initially in contact with the glass tile and, together with the sabot, it was given an initial velocity according to the experimental tests using the Initial_Velocity_Node card. The parameters evaluated by Abouridouane et al. [13] were adopted here, as listed in Table 5.

Table 5. JC model parameters for carbon steel projectile

Parameter	Notation	Value	Units
Density	ρ_0	7850	Kg/m^3
Poisson's Ratio	ν	0,31	
Elastic Modulus	E	186	GPa
-	A	546	MPa
-	B	487	MPa
-	n	0,25	
-	C	0,015	
Effective plastic strain rate	*EPS0*	1	

Also, Tied_Surface_to_Surface contact condition was used to attach the projectile to its polymeric sabot, while for the contact between the end of the supports and the glass tile as well as the contact between the tile and the projectile, Automatic_Surface_to_Surface option was selected. In the case of FEM-SPH, also other conditions were set. In fact, apart from the conversion of solid elements into SPH particles, the SPH part was put in contact using the Automatic_Nodes_to_Surface contact condition with all the parts initially in contact with the tile (projectile and ends of the supports).

4.2. Results and discussion

The effect of the impact velocity was explored as a consequence of the different modelling choices. The velocity history of the projectile for the two simulation techniques is shown in Figure 8. As can be seen, in general the FEM-SPH is able to more accurately approximate the experimental results. Specifically, a particularly higher residual speed is obtained for CEM with respect to the experimental values. The Aluminosilicate glass tile replicated by CEM seems to be unable to sufficiently slow down the projectile, absorbing its kinetic energy. Such discrepancy from the experimental results tends to decrease if the impact velocity increases. Also, for both techniques a wavy trend due to the formation of longitudinal mechanical waves on the bullet after the impact is exhibited in the curves. This behaviour is replicated in both simulation techniques with the same phase.

The two simulation techniques were compared in terms of the glass tile's failure mode as well. This analysis highlighted some important differences between the obtained results. First of all, the graphical representation of a crack using CEM immediately shows the difficulty in finding a suitable representation of the failure pattern, because with this technique the crack path is the result of the deletion of the cohesive elements that have a null thickness and, consequently, don't leave any significant and visible empty space in the model. In Figure 9 the failure process is shown both with half-shaded solid elements, in order to make the deletion of cohesive elements visible, and only from the cohesive elements point of view.

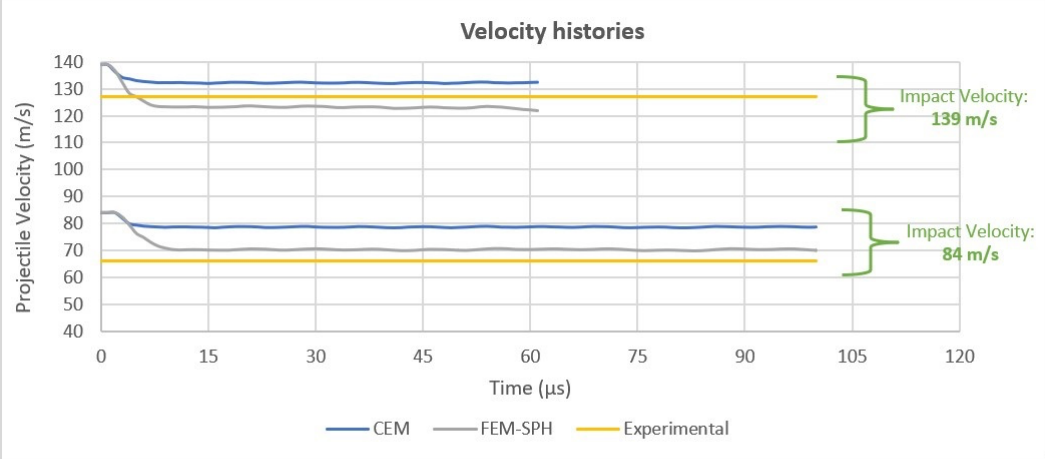

Impact Velocity (m/s)	Residual Velocity (m/s)		
	Experimental	CEM	FEM-SPH
84	66	79 (+19,6%)	69 (+4,5%)
139	127	132 (+3,9%)	123 (-3,1%)

Figure 8. Summary of the obtained velocity histories for CEM and FEM-SPH models at different impact velocities.

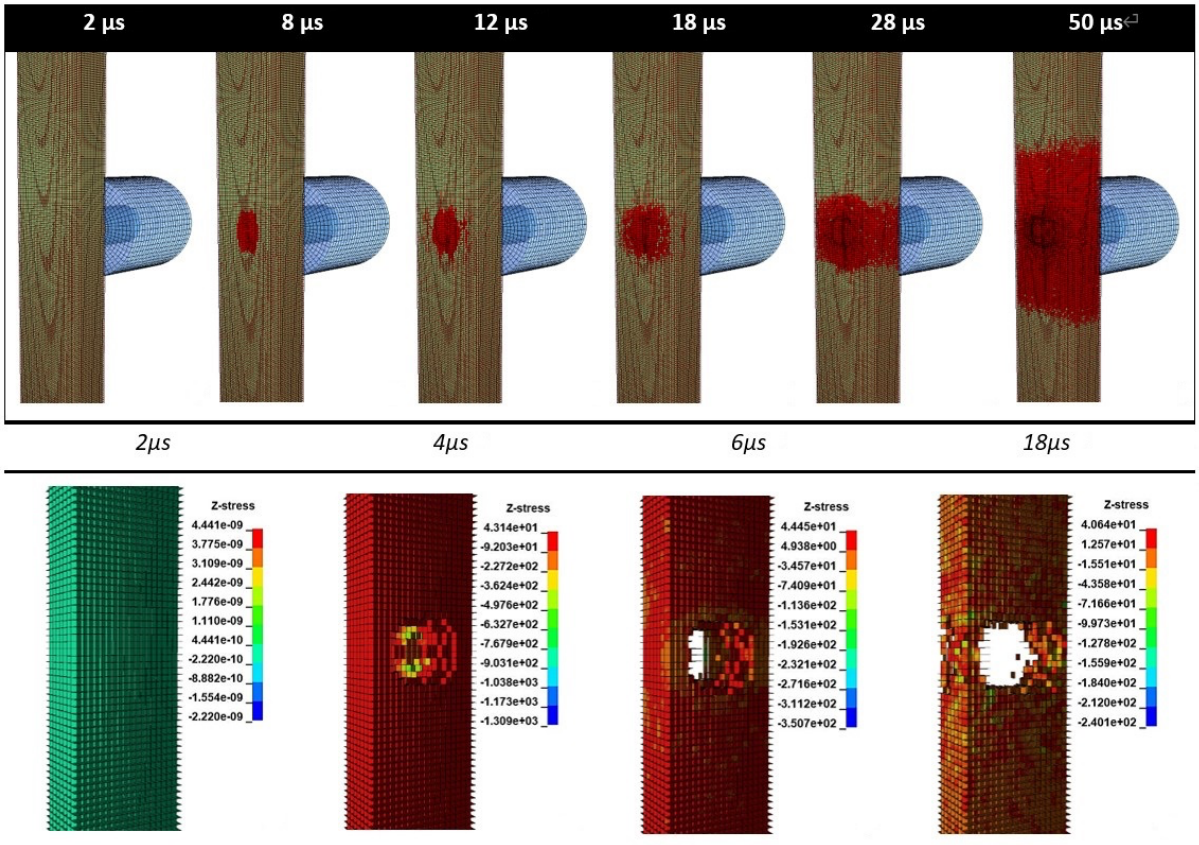

Figure 9. Above: Failure progressions for 1mm mesh impact CEM models. Cohesive elements are coloured in green. Below: Deletion progression of cohesive elements of the glass tile with an indication about the level of stress of cohesive elements exiting from the plane.

During the experiments, an ultra-high-speed camera with a frame rate of 500000 fps (time interval 2μs between neighbouring images) was used to capture the dynamic fragmentation process of the glass tiles. Due to the transparency property of glass, intact specimens were black in the image. When cracks initiated, the light from the flash was reflected by the newly formed crack surface and detected by the camera. In Figure 10 a comparison between the mid-section view of the failure is reported for the CEM and FEM-SPH models, while in Figure 11 an improved graphical representation shows the failure process using the Damage quantity defined for the JH2 model for different instants of time.

As can be seen from Figure 10, the FEM-SPH model provides a better failure mode, especially in terms of extent of the deformation of the broken glass tile. In fact, CEM is hardly able to transfer the loads for a long distance, and, rather, cohesive elements fail locally where the solicitation is applied. The consequence of this behaviour in the simulation of a ballistic impact is the formation of a circular hole in correspondence with the passage of the projectile, as visible clearly in Figure 11.

The incapability of CEM to transfer the loads far from the impacted area is reflected also by the fact that immediately after the impact, no visible crack or cohesive elements deletion is shown far from the projectile. Instead, the deletion of elements starts from the impacted area and then proceeds towards the extremes of the glass tile. Instead, in the case of FEM-SPH model, a larger fragmentation of the glass target follows the initial formation of a circular damage, and, as in the experimental images, some cracks are formed also far from the impacted area.

Accordingly, in CEM a smaller portion of the target material is solicited during the impact and, consequently, a smaller amount of kinetic energy is absorbed by the impacted material. This fact is consistent with the higher residual velocity that was obtained previously in the residual velocity plot for the CEM model with respect to FEM-SPH.

From a purely graphical point of view, also, though an improvement in the representation was obtained by adjusting the transparency of solid elements, CEM never allows a clear visualization of the crack propagation. Accordingly, also in the visual aspect of the failure process, the FEM-SPH method is more reliable both far and close to the impacted area.

Finally, one last comparison between the two techniques can be made in terms of computational time. With a 4 cores and 8 logical processors CPU @3.4GHz, the FEM-SPH model for ballistic impact simulation took about 1 hour and 12 minutes to process the data, while for CEM the same quantity took about 50 minutes if the mesh size was chosen equal to 0,5 mm (the same used also for the FEM-SPH model). Thus, it is possible to conclude that the reliability shown by the FEM-SPH technique requires a higher computational time than CEM.

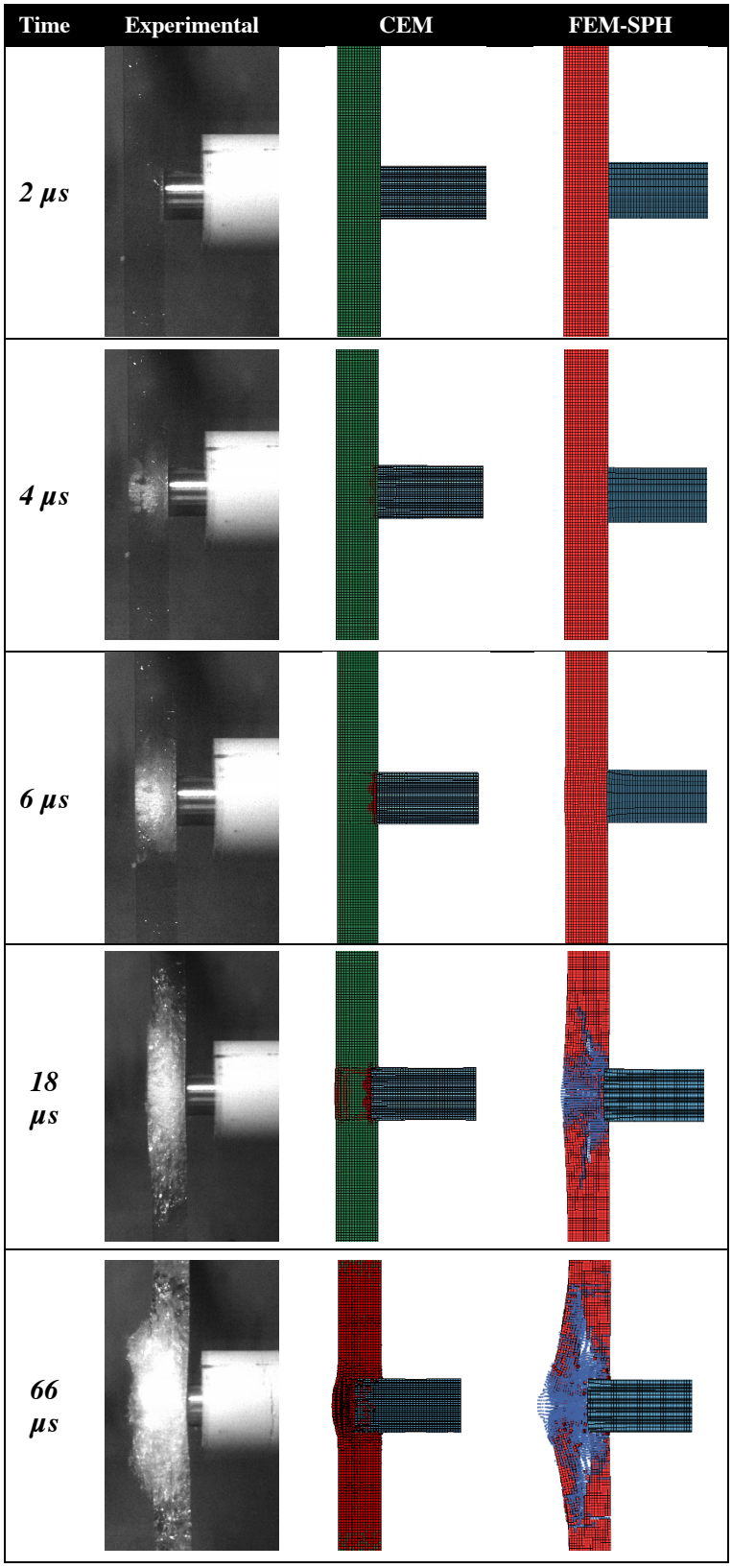

Figure 10. Mid-section view of the failure patterns of CEM (cohesive elements are coloured in green) and FEM-SPH models.

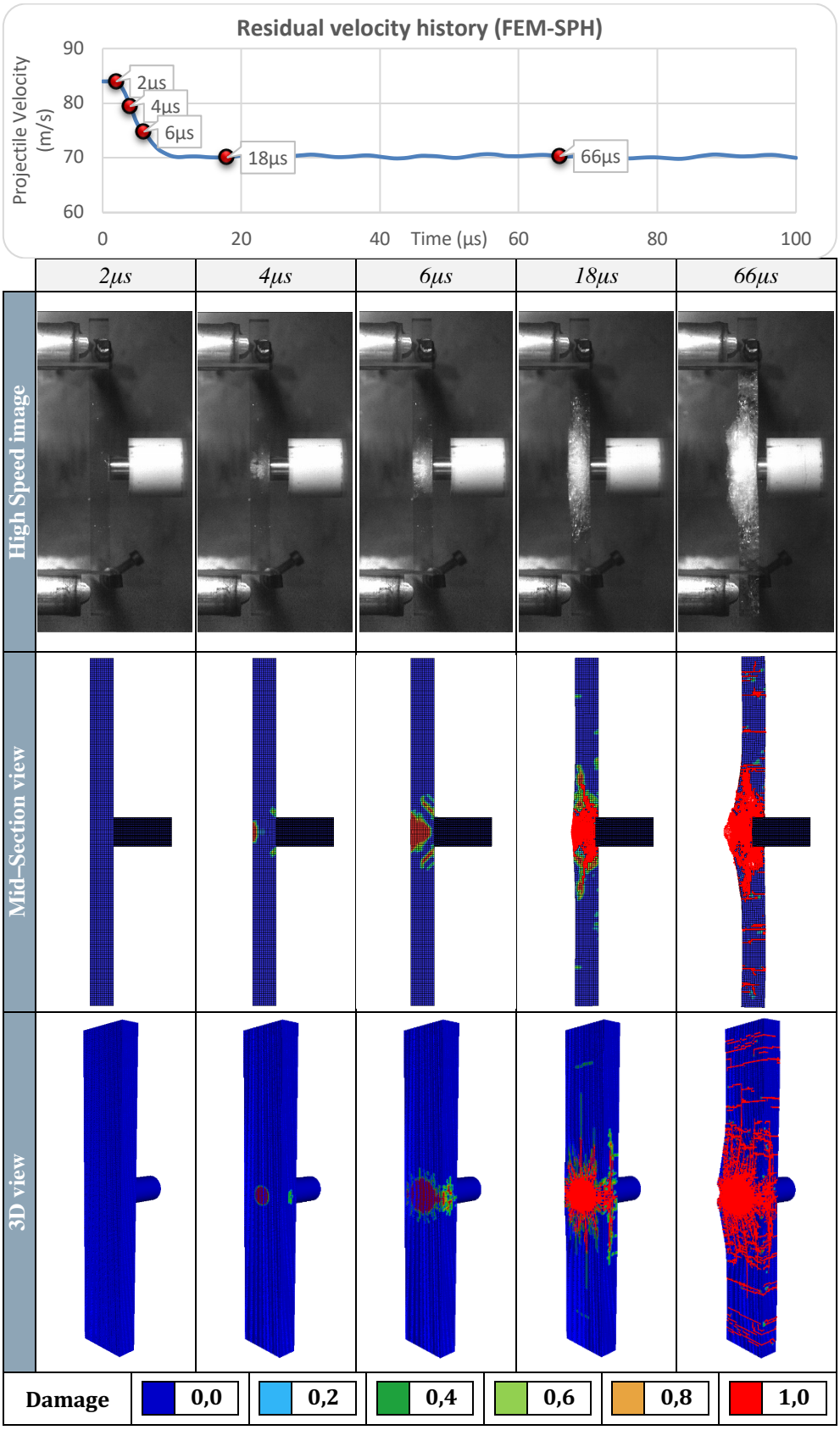

Figure 11. Failure progression of 84 m/s FEM-SPH model in terms of Damage.

5. Conclusions

In this paper two different simulation approaches (CEM and FEM-SPH) were employed in LS-Dyna and tested in the prediction of the mechanical and failure behaviour of Aluminosilicate glass. Two loading situations were considered: quasi-static and dynamic tests and impact loading conditions.

In the first case, in general both simulation techniques demonstrated to be valid and suitable to obtain reasonable results. In fact, under both tensile and compressive loading conditions, good results were obtained, and it was always possible to find solutions to all the characteristic problems that arose (like stress concentration). One interesting analogy between the two methods is that both techniques are able to predict the strain rate effect in compression, but not in tension. However, this fact is the result of two different and totally independent causes. In particular, CEM provided good strain rate sensitivity without inserting any direct correlation between the mechanical behaviour of the model and the loading rate. Conversely, in the other technique proper tuning of the strain rate sensitivity of the model needs to be performed. In fact, an advantage of CEM is in general the smaller number of parameters the model relies on, with respect to FEM-SPH method, that requires ad-hoc and time-consuming tuning processes.

As far as the ballistic impact simulations are concerned, in general terms the difference in the results between CEM and FEM-SPH increases. In fact, the reported results evidenced that FEM-SPH method behaves better than CEM practically always in terms of correctness of the results and capability to reproduce the crack aspect of the experimental specimen. However, this technique has a drawback which is the increased required computational time.

To conclude, none of the two simulation techniques demonstrated to be totally convenient with respect to the other, since both evidenced weaknesses and strengths. However, the simulation of impacts developed by the FEM-SPH approach and JH2 constitutive model provide better results, both in quantitative (residual speed) and qualitative terms (failure pattern).

References

[1] Wang Z, Ma D, Suo T, Li Y and Manes A 2021 *Int. J. Mech. Sci.* **196**
[2] Ma D, Esmaeili A, Manes A, Sbarufatti C, Jiménez-Suárez A, Giglio M and Hamouda A M 2020 *Mech. Mater.* **140** 103214
[3] Wang Z, Fu J and Manes A 2021 *Theor. Appl. Fract. Mech.* **111**
[4] Zhang W 2019 *Numerical Representation of Crack Propagation within the Framework of Finite Element Method Using Cohesive Zone Model* (University of Cincinnati)
[5] Wu X, Wang G, Li G, Han W, Sun S, Zhang S and Bi W 2020 *Symmetry (Basel).* **12** 1314
[6] Pandolfi A and Ortiz M 2002 *Eng. Comput.* **18** 148–59
[7] Jiang H and Meng D 2018 *Eng. Fract. Mech.* **199** 280–93
[8] Xu X, Chen S, Wang D and Zang M 2020 *Theor. Appl. Fract. Mech.* **108** 102660
[9] Liu M B and Liu G R 2010 *Arch. Comput. methods Eng.* **17** 25–76
[10] Liu G-R and Liu M B 2003 *Smoothed particle hydrodynamics: a meshfree particle method* (World scientific)
[11] Vignjevic R and Campbell J 2009 *Predictive modeling of dynamic processes* (Springer) pp 367–96
[12] Jankowiak T and Łodygowski T 2013 *Bull. Polish Acad. Sci. Tech. Sci.* 111–21
[13] Abouridouane M, Klocke F, Lung D and Adams O 2012 *CIRP Ann.* **61** 71–4
[14] Wang Z, Ren T, Suo T and Manes A 2021 *Thin-Walled Struct.* **165**
[15] Johnson G R and Holmquist T J 1994 *AIP conference proceedings* vol 309 (American Institute of Physics) pp 981–4
[16] Wang Z, Li Y, Ma D, Li Y, Suo T and Manes A 2022 *Submitt. to Mech. Mater.*